

## Optical properties of highly reduced $\text{SrTiO}_{3-x}$

D. A. Crandles, B. Nicholas, and C. Dreher

*Department of Physics and Astronomy, Franklin and Marshall College, Lancaster, Pennsylvania 17604-3003*

C. C. Homes

*Department of Physics, Brookhaven National Laboratory, Upton, New York 11973-5000*

A. W. McConnell and B. P. Clayman

*Department of Physics, Simon Fraser University, Burnaby, British Columbia, Canada V5A 1S6*

W. H. Gong and J. E. Greedan

*Department of Chemistry and Brockhouse Institute for Materials Research, McMaster University, Hamilton, Ontario, Canada L2S 4M1*

(Received 17 December 1998)

The reflectance of highly reduced  $\text{SrTiO}_{3-x}$  has been studied in samples where the carrier concentration—or oxygen-vacancy density—varies from about  $10^{18}$  to  $10^{21}$   $\text{cm}^{-3}$ . Several phonon modes are strongly influenced by oxygen-vacancy density. Oxygen reduction induces a mid-infrared band whose oscillator strength scales with carrier density. In highly reduced samples, a weakly localized plasmon mode develops. [S0163-1829(99)10919-6]

### I. INTRODUCTION

There is a substantial body of literature on the metal-insulator transition produced by chemically doping insulating metal oxides.<sup>1-6</sup> This problem has been of general interest ever since the discovery of the high-temperature superconductors which are produced by chemically doping antiferromagnetic insulators. This work is a study of the dependence of the far- and mid-infrared optical reflectance of the  $\text{SrTiO}_{3-x}$  system on the density of oxygen vacancies. The work complements earlier optical studies of reduced  $\text{SrTiO}_{3-x}$  (Refs. 7-9) and of Nb-doped  $\text{SrTiO}_3$  (Ref. 10). Four samples were prepared to span a four decade variation in dc conductivity which, to a first approximation, is proportional to the oxygen-vacancy density. In highly disordered samples, the vacancy density is greater than the conductivity measurements predict, since some of the donated electrons are localized due to disorder. Disorder has a marked influence on the optical properties of the  $\text{SrTiO}_{3-x}$  system both on the phonon modes and on the plasmon mode that develops in highly reduced samples.

### II. SAMPLES

Three of the samples were polished (100)  $\text{SrTiO}_3$  substrates purchased from Atomergic Chemicals (AC). The substrates were subjected to different reducing treatments, listed in Table I, to achieve different oxygen-vacancy densities. The sample with the largest number of oxygen vacancies and hence the most disorder was a polished, unoriented  $\text{SrTiO}_{2.72}$  crystal prepared by radio-frequency induction as explained in a previous publication.<sup>11</sup> Throughout this paper, the samples will be referred to by the carrier concentration rather than the oxygen-vacancy density since the former can be estimated using dc resistivity measurements. Measured using the Van der Pauw technique using silver paint contacts, the dc resis-

ivities of the samples are summarized in Table I. The carrier concentrations listed in Table I are based on the direct correlation between the room-temperature resistivity and the carrier concentration which is illustrated in Fig. 1. The calibration data in this figure include several different doping methods: reduction, Nb substitution for Ti, and La substitution for Sr. The  $\text{SrTiO}_{3-x}$  system exhibits a metal-insulator transition<sup>7</sup> for carrier densities greater than about  $10^{18}$   $\text{cm}^{-3}$ . Hence, all four samples are on the metallic side of the metal-insulator transition and exhibit positive temperature coefficients of resistivity.

### III. RESULTS AND DISCUSSION

#### A. Reflectance data

The reflectance was measured at several temperatures using an *in situ* evaporation technique.<sup>16</sup> Figure 2 shows the oxygen vacancy and temperature dependence of the far-infrared reflectance spectra for three of the samples. One can make several observations. The first is that the shapes of the three high-reflectance bands change as the number of free carriers (oxygen vacancies) increases. Secondly, temperature has a more pronounced effect on the two highest-frequency modes when the carrier density is large. The third observation is that the reflectance at around  $900$   $\text{cm}^{-1}$  increases systematically with increasing carrier density. Figure 3 presents the temperature dependence of the reflectance of  $\text{SrTiO}_{2.72}$ . In this sample, the oxygen-vacancy density is large enough that a plasmon mode is well developed, leading to screening of the phonon modes.

#### B. Vibrational modes

The  $\Gamma$ -point transverse optical modes are all affected by oxygen reduction as seen in Fig. 4, which illustrates the dependence of the room-temperature real optical conductivity

TABLE I. Preparation and characterization of the Atomegic Chemicals polished (100)  $\text{SrTiO}_3$  substrates (AC) as well as the  $\text{SrTiO}_{2.72}$  crystal. Carrier density is estimated using the room-temperature resistivities  $\rho_{dc}$  (300 K) and Fig. 1.

Sample	$\rho_{dc}$ (300 K)(m $\Omega$ cm)	$n(\text{cm}^{-3})$	Reducing treatment
AC-1	500	$2.0 \times 10^{18}$	$\text{H}_2$ -1050 °C-3 h
AC-2	70	$1.4 \times 10^{19}$	$\text{H}_2$ -1050 °C-16 h
AC-3	6.4	$1.6 \times 10^{20}$	Ti metal-1000 °C-75 h
$\text{SrTiO}_{2.72}$	0.6	$2.4 \times 10^{21}$	

on carrier density. The data for the oxygen-reduced samples were obtained by Kramers-Kronig analysis of the reflectance, with appropriate high- and low-frequency extrapolations. The data for stoichiometric  $\text{SrTiO}_3$  were generated from the dielectric function given in Ref. 10. The two main features in Fig. 4 that must be explained are the hardening and broadening of the transverse modes with increased free-carrier density. In an attempt to distinguish between the effects of disorder and carrier density, data for Nb-doped  $\text{SrTiO}_3$  (Ref. 10) are also included in the figure. The carrier concentration for  $\text{SrTiO}_3(\text{Nb})$  was estimated by using the calibration of Fig. 1, taking the zero-frequency limit of  $1/\sigma(\omega) = 1.4 \text{ m}\Omega \text{ cm}$  as the dc resistivity.<sup>10</sup> The width of the transverse modes in the oxygen-reduced samples systematically increases with decreasing resistivity. However, the width of the peaks in the Nb-doped sample where  $n = 7.0 \times 10^{20} \text{ cm}^{-3}$  is less than the width of the peaks of the oxygen-reduced sample where  $n = 1.6 \times 10^{20} \text{ cm}^{-3}$ . This must be due to the greater disorder associated with oxygen vacancies compared with substitutional impurities.

Consider the hardening of the lowest-frequency mode with increasing carrier density. This has been previously observed by both neutron scattering and temperature-derivative Raman spectroscopy.<sup>17</sup> The frequency shift of the low-frequency mode with carrier density is remarkable. Whereas the mode appears at  $89 \text{ cm}^{-1}$  in undoped material<sup>10</sup> it appears at  $156 \text{ cm}^{-1}$  for the most highly reduced sample shown in Fig. 4. In comparison, the maximum peak frequency observed by Bäuerle *et al.* was roughly  $145 \text{ cm}^{-1}$

for a sample where the Hall carrier density was  $1.6 \times 10^{21} \text{ cm}^{-3}$ . Note that in the Nb-doped sample, the frequency shift of the low-frequency mode is smaller than the shift of an oxygen-reduced sample where  $n = 1.6 \times 10^{20} \text{ cm}^{-3}$ . This is evidence that some other mechanism besides free-carrier screening is the primary cause of the frequency shift. Bäuerle *et al.* suggested that oxygen-vacancy-induced changes in both long-range dipole-dipole and short-range forces produce the frequency shift<sup>17</sup> in the low-frequency mode. This is a likely explanation for the shift in all the TO modes.

Structural considerations should also be addressed. The sample where  $n = 2.4 \times 10^{21} \text{ cm}^{-3}$  exhibits a small tetragonal structural distortion.<sup>11</sup> Figure 4 indicates that the distortion is too small to induce mode splitting, which could have been observed since measurements were made on a low-symmetry crystal face.

The effect of carrier density on the LO modes can be explored using the dielectric loss function, shown in Fig. 5. Note that the peaks in the loss function shift to higher frequency as the carrier density increases. In their study of Nb-doped  $\text{SrTiO}_3$ , Gervais *et al.* proposed a model in which the shift is due to increased plasma frequency; as the carrier density increases, the free-carrier plasma frequency also increases,<sup>10</sup> which causes the peaks in the dielectric loss function  $\text{Im}[-1/\tilde{\epsilon}(\omega)]$ , where  $\tilde{\epsilon}(\omega) = \epsilon_1(\omega) + i\epsilon_2(\omega)$  is the complex dielectric function, to move to higher frequency. While it is true that adding a free-carrier term to any simple model dielectric function causes both the peaks in the dielec-

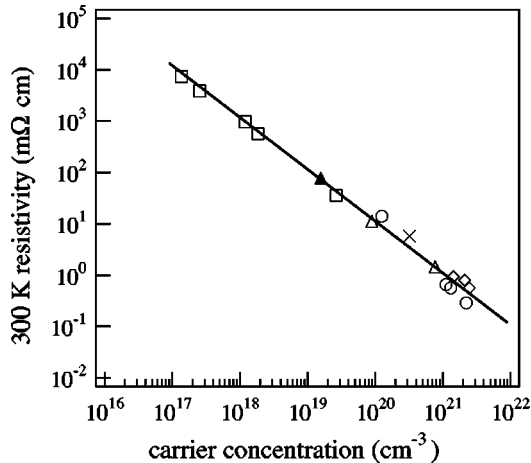


FIG. 1. A calibration curve for room-temperature dc resistivity versus Hall carrier concentration. A single band model is assumed. Squares, Ref. 12; circles, Ref. 13; open triangles, Ref. 8; filled triangle, Ref. 14; cross Ref. 15; and diamonds, Ref. 11.

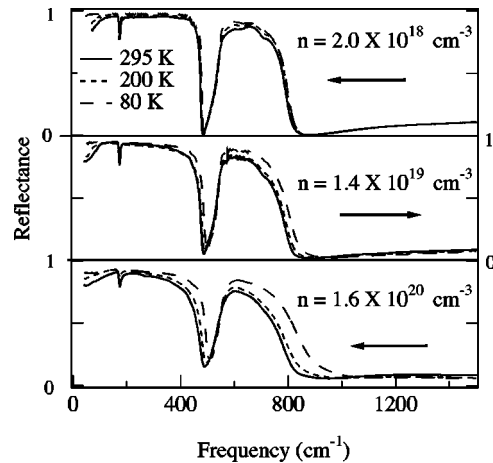


FIG. 2. Temperature and doping dependence of far-infrared reflectance spectrum of reduced  $\text{SrTiO}_3$  samples. The reflectance is shown for three temperatures: 295 K (solid curve), 200 K (dotted), and 80 K (dashed), and for the three different carrier concentrations.

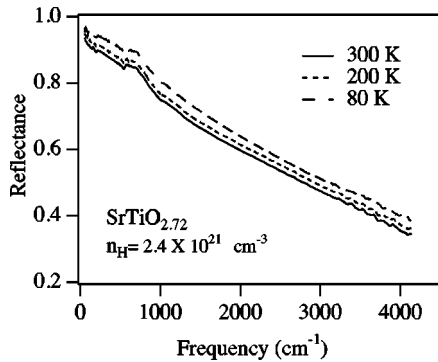


FIG. 3. Reflectance spectrum of  $\text{SrTiO}_{2.72}$  at three different temperatures: 295 K (solid curve), 200 K (dotted), and 80 K (dashed).

tric loss function to shift to higher frequency and the phonon-related reflectance bands to widen, there are problems with the simple model. For example, it was also proposed that this mechanism is responsible for the temperature dependence of the high-frequency reflectance bands observed in Fig. 2. In order to account for the increased widths of the bands at low temperature within this simple model, it is necessary for the plasma frequency to increase by up to a factor of 2 as the temperature decreases from 300 to 78 K (Ref. 10). However, a study of the temperature dependence of the optical conductivity of  $\text{SrTiO}_{2.72}$  where  $n_H = 2.4 \times 10^{21} \text{ cm}^{-3}$  does not support this hypothesis. A Kramers-Kronig analysis was performed on the reflectance data of Fig. 3, which yields the real part of the optical conductivity shown in Fig. 6. According to the conductivity sum rule,<sup>22</sup> the plasma frequency is related to the integrated optical conductivity according to  $\omega_p^2 = \frac{1}{8} \int_0^\infty \sigma(\omega) d\omega$ . In practical terms, the upper limit of this integral is the lower-frequency limit of the interband transitions. An examination of Fig. 6 reveals that the plasma frequency does not change significantly be-

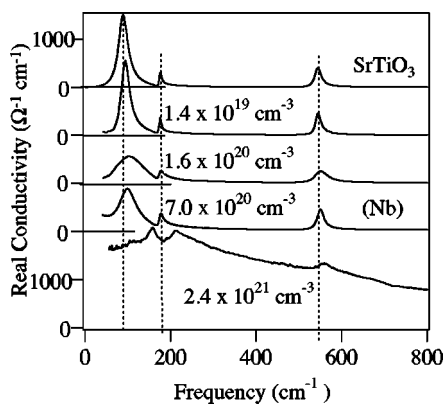


FIG. 4. Variation of the room-temperature real optical conductivity with carrier concentration. The figure compares the optical conductivity of stoichiometric  $\text{SrTiO}_3$  with three oxygen-reduced samples and one Nb-doped sample (Nb). The curve for the Nb-doped sample is generated from the dielectric function and parameters discussed in Ref. 10. The carrier concentration for the Nb-doped sample was estimated by using the calibration of Fig. 1 with zero-frequency  $1/\sigma(\omega \rightarrow 0) = 1.4 \text{ m}\Omega \text{ cm}$  as the dc conductivity. For clarity, the second curve ( $n = 7 \times 10^{20} \text{ cm}^{-3}$ ) is offset by  $2000 \text{ }\Omega^{-1} \text{ cm}^{-1}$ , while the other curves are offset successively by  $1000 \text{ }\Omega^{-1} \text{ cm}^{-1}$ .

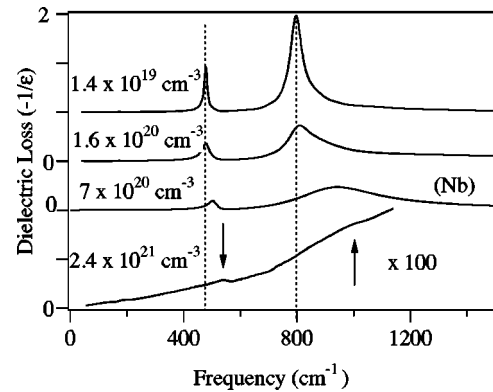


FIG. 5. Variation of the room-temperature dielectric loss function with carrier concentration. The curves for the oxygen-reduced samples were determined by Kramers-Kronig analysis. The figure compares the loss function of three oxygen-reduced samples as well as a Nb-doped sample (Nb). (See the caption to Fig. 4 for an explanation of how the carrier density was estimated for the Nb-doped sample.) This latter spectrum was generated from the dielectric function and parameters discussed in Ref. 10.

tween 80 and 295 K. It certainly does not change by a factor of 2 to 4. One can conclude that a satisfactory explanation of the temperature dependence of the reflectance of  $n$ -type  $\text{SrTiO}_3$ —which will probably involve electron-phonon coupling—is yet to be found.

### C. Plasmon mode

An interesting aspect of Fig. 6 is the non-Drude-like depressed low-frequency conductivity, seen most clearly in the inset. This can be attributed to disorder-induced localization which has also been observed in radiation-damaged  $\text{YBa}_2\text{Cu}_3\text{O}_{6.95}$  (Ref. 18) and in the conducting polymer polyaniline protonated with camphor sulfonic acid.<sup>19</sup> Localization effects are expected in  $\text{SrTiO}_{2.72}$  due to the huge number of oxygen vacancies, and the fact that there is some  $\text{O}(2p)$  character to states near the Fermi level. Figure 6 also

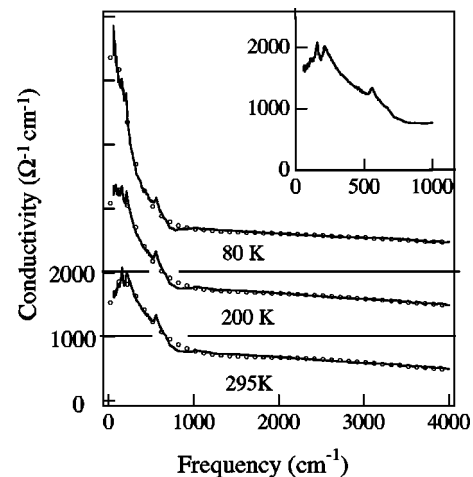


FIG. 6. Real part of the optical conductivity of  $\text{SrTiO}_{2.72}$  (solid curves). Each successive curve has been offset by  $1000 \text{ }\Omega^{-1} \text{ cm}^{-1}$  for clarity. The open circles are predictions of Eq. (1) using the parameters listed in Table II. The inset shows the optical conductivity at low frequency at 295 K.

TABLE II. Parameters for fits of Eq. (1) to the real part of the optical conductivity of SrTiO<sub>2.72</sub>. Table entries are in cm<sup>-1</sup>, except for  $k_F l$ , which is dimensionless.

$T$ (K)	$\omega_p$	$\Gamma$	$k_F l$	$\omega_{om}$	$\Gamma_m$	$\omega_{pm}$
80	7300	230	2.2	2240	6600	14 300
200	7300	350	1.8	2340	5600	13 500
300	7300	450	1.6	2550	5200	12 600

shows that a mid-infrared absorption exists in addition to the plasmon mode. One model for the real electronic conductivity of SrTiO<sub>2.72</sub> is given in Eq. (1) below, and consists of the sum of a localization-modified Drude contribution<sup>20</sup> and a mid-infrared Lorentzian. The weakly localized plasmon mode parameters are the strength ( $\omega_p$ ), scattering rate ( $\Gamma$ ), and a localization parameter ( $k_F l \approx 1$  when the electrons become localized). The Fermi wave vector is  $k_F$ , the mean free path is  $l$ , while  $C$  is a constant of order 1. The center frequency, width, and strength of the mid-infrared Lorentzian are  $\omega_{om}$ ,  $\Gamma_m$ , and  $\omega_{pm}$ , respectively.

$$\sigma_1(\omega) = \frac{\omega_p^2 \Gamma}{60(\Gamma^2 + \omega^2)} \left\{ 1 - \frac{C}{(k_F l)^2} \left[ 1 - \left( \frac{3\omega}{\Gamma} \right)^{1/2} \right] \right\} + \frac{\omega_{pm}^2 \Gamma_m \omega^2}{60[\Gamma_m^2 \omega^2 + (\omega^2 - \omega_{om}^2)^2]} \quad (1)$$

Because of the presence of the mid-infrared band, it is impossible to use the conductivity sum rule to obtain the plasma frequency. The fitting procedure was first to find  $\omega_p$ ,  $\Gamma$ , and  $k_F l$  for the 295 K spectrum. For the other temperatures,  $\omega_p$  was fixed while the other parameters were allowed to vary in a way which is consistent with the temperature independence of the Hall coefficient.<sup>11</sup>

The fitting parameters are listed in Table II, while comparisons of the experimental optical conductivity and the model can be seen in Fig. 6. There is reasonable agreement between the zero-frequency limit of the model conductivity and the measured dc conductivity at all temperatures. Assuming that  $k_F = \pi/2a$  where  $a$  is 5.5 Å, then the mean-free path is of the order of 10 Å at 80 K, which is comparable to the average interimpurity spacing of 6 Å in SrTiO<sub>2.72</sub>. The temperature dependence of  $k_F l$  is interesting since it suggests that electron-phonon coupling as well as disorder is contributing to the localization of the carriers. If static disorder was the only localizing effect, then  $k_F l$  would be a constant. The shift of the peak in the localized plasmon mode towards zero frequency is curiously similar to that observed in the bad metal SrRuO<sub>3</sub> (Ref. 21). The real part of the optical conductivity of high-quality, low residual-resistivity, thin films of SrRuO<sub>3</sub> exhibits a finite frequency peak. It was suggested that dynamic localization rather than static disorder was the origin of this feature.

#### D. Mid-infrared absorption

If the carrier density is large enough, the mid-infrared reflectance of  $n$ -type SrTiO<sub>3</sub> begins to exhibit structure, as is shown in Fig. 7. Structure in the mid-infrared transmission spectrum in reduced SrTiO<sub>3-x</sub> has been observed

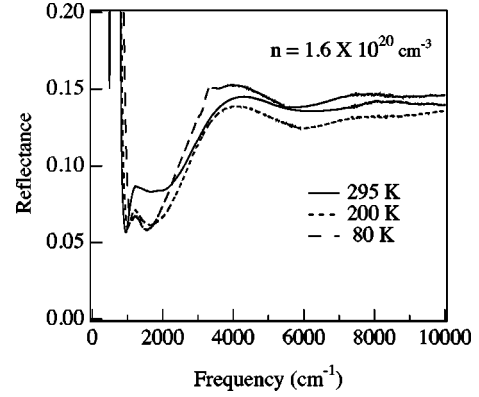


FIG. 7. Temperature dependence of the mid-infrared reflectance of sample AC-3 for which  $n = 1.6 \times 10^{20} \text{ cm}^{-3}$ .

previously<sup>7,9</sup> but the origin of the different components comprising the mid-infrared band is still controversial. The mid-infrared absorption is the reason for the systematic increase in reflectance near 900 cm<sup>-1</sup> that one can observe in Fig. 2. The doping-induced mid-infrared band and electrical transport are linked. Many years ago it was suggested that the charge carriers in SrTiO<sub>3</sub> are small polarons and that the mid-infrared absorption was due to absorption by small polarons.<sup>23</sup> However, the relative temperature independence of the mid-infrared band seen in Fig. 6 does not agree with this hypothesis. Others have suggested that the charge carriers in SrTiO<sub>3</sub> are large polarons. Large polarons have a temperature-independent optical signature<sup>25</sup> that is, however, much narrower than the rather broad feature shown in Fig. 6.

It is interesting to compare the mid-infrared absorption in SrTiO<sub>2.72</sub> with a previous study of the mid-infrared band in SrTiO<sub>3-x</sub> (Ref. 7). In that study, an absorption at roughly the same frequency as that listed in Table II was observed to scale with the dc conductivity for samples with carrier densities ranging from 10<sup>14</sup> to 10<sup>18</sup> cm<sup>-3</sup> (Ref. 7). Remarkably, the strength of the mid-infrared band in SrTiO<sub>2.72</sub> where  $n = 2.4 \times 10^{21} \text{ cm}^{-3}$  is roughly what would have been predicted by this scaling relation which now may be assumed to hold over seven orders of magnitude in free-carrier density. Calvani *et al.* suggested that the mid-infrared absorption was due to intervalley carrier scattering.<sup>7</sup> This assumes a rigid-band model of doping which is probably not applicable. Recent calculations by Shanthi and Sarma have demonstrated that oxygen clustering in heavily oxygen-reduced SrTiO<sub>3-δ</sub> produces midgap states.<sup>24</sup> Thus, the mid-infrared Lorentzian used in the model conductivity of Eq. (1) could account for transitions between the midgap states and the conduction band. The overlap in frequency of the plasmon mode and the mid-infrared mode precludes attaching too much importance to the small and systematic temperature dependence in the mid-infrared parameters listed in Table II.

#### IV. CONCLUSIONS

The reflectance of highly reduced SrTiO<sub>3-x</sub> has been studied in samples where the oxygen-vacancy or free-carrier concentration varies from 10<sup>18</sup> to 10<sup>21</sup> cm<sup>-3</sup>. As well as the three perovskite infrared active phonons, free-carrier and mid-infrared contributions must be considered to successfully model the reflectance and optical conductivity in

samples with large carrier concentrations. It has been shown that the presence of oxygen vacancies affects the reflectance of SrTiO<sub>3</sub> in several ways: The TO modes all harden and broaden with doping. It was argued that these effects are due primarily to oxygen-vacancy-related disorder which changes both the short-range and long-range Coulomb forces. The LO modes are affected as well. The temperature shift of the two high-frequency peaks in the loss function  $\text{Im}[-1/\tilde{\epsilon}(\omega)]$  which is associated with the changing width of the reflectance bands is not completely understood. The eventual explanation of the temperature dependence of the reflectance in *n*-type SrTiO<sub>3</sub> will most likely involve electron-phonon coupling, and may be of significance in elucidating the transport properties of *n*-type SrTiO<sub>3</sub>.

It has also been shown that the oxygen-vacancy density contributes to weak localization of the plasmon mode in highly doped SrTiO<sub>2.72</sub> and that the localization parameter is

temperature dependent. This may be an indication that phonons as well as static disorder play a role in the weak localization of the carriers in highly oxygen-deficient SrTiO<sub>3-x</sub>.

#### ACKNOWLEDGMENTS

D.A.C. acknowledges financial assistance in the form of start-up funds from Franklin and Marshall College and Research Corporation Grant No. CC4141. A.M. wishes to thank SFU for financial support. The authors are grateful for helpful conversations with D. Emin and R.N. Bhatt. The work was also supported by the National Science and Engineering Research Council of Canada and the Department of Energy, Division of Materials Research, under Contract No. DE-AC02-98CH10886.

- 
- <sup>1</sup>S. Uchida, T. Ido, H. Takagi, T. Arima, Y. Tokura, and S. Tajima, *Phys. Rev. B* **43**, 7942 (1991).
- <sup>2</sup>S. L. Cooper, G. A. Thomas, J. Orenstein, D. H. Rapkine, A. J. Millis, S-W. Cheong, and A. S. Cooper, *Phys. Rev. B* **41**, 11 605 (1990).
- <sup>3</sup>M. Reedyk, T. Timusk, J. S. Xue, and J. E. Greedan, *Phys. Rev. B* **45**, 7406 (1992).
- <sup>4</sup>I. Terasaki, T. Nakahashi, S. Takebayashi, A. Maeda, and K. Uchinokura, *Phys. Rev. B* **43**, 551 (1991).
- <sup>5</sup>T. Ido, K. Magoshi, H. Eisaki, and S. Uchida, *Phys. Rev. B* **44**, 12 094 (1991).
- <sup>6</sup>T. Katsufuji, Y. Okimoto, and Y. Tokura, *Phys. Rev. Lett.* **75**, 3497 (1995).
- <sup>7</sup>P. Calvani, M. Capizzi, F. Donato, S. Lupi, P. Maselli, and D. Peschiaroli, *Phys. Rev. B* **47**, 8917 (1993).
- <sup>8</sup>A. S. Barker, in *Proceedings of the International Colloquium on Optical Properties and Electronic Structure of Metals and Alloys*, edited by F. Abelès (North-Holland, Amsterdam, 1966).
- <sup>9</sup>C. Lee, J. Destry, and J. L. Brebner, *Phys. Rev. B* **11**, 2299 (1975).
- <sup>10</sup>F. Gervais, J-L. Servoin, A. Baratoff, J. G. Bednorz, and G. Binnig, *Phys. Rev. B* **47**, 8187 (1993).
- <sup>11</sup>Wenhe Gong, H. Yun, Y. B. Ning, J. E. Greedan, W. R. Datars, and C. V. Stager, *J. Solid State Chem.* **90**, 320 (1991).
- <sup>12</sup>O. N. Tufte and P. W. Chapman, *Phys. Rev.* **155**, 796 (1967).
- <sup>13</sup>M. Higuchi, K. Aizawa, K. Yamaya, and K. Kodaira, *J. Solid State Chem.* **92**, 573 (1991).
- <sup>14</sup>H. P. R. Frederiske and W. R. Hosler, *Phys. Rev.* **161**, 822 (1967).
- <sup>15</sup>K. Uematsu, O. Sakurai, N. Mizutani, and M. Kato, *J. Mater. Sci.* **19**, 3671 (1984).
- <sup>16</sup>C. C. Homes, M. Reedyk, D. A. Crandles, and T. Timusk, *Appl. Opt.* **32**, 2976 (1993).
- <sup>17</sup>D. Bäuerle, D. Wagner, M. Wohlecke, B. Dorner, and H. Kraxenberger, *Z. Phys. B* **38**, 335 (1980).
- <sup>18</sup>D. N. Basov, A. V. Puchkov, R. A. Hughes, T. Strach, J. Preston, and T. Timusk, *Phys. Rev. B* **49**, 12 165 (1994).
- <sup>19</sup>Kwanghee Lee, A. J. Heeger, and Y. Cao, *Phys. Rev. B* **48**, 14 884 (1993).
- <sup>20</sup>N. F. Mott, *Metal-Insulator Transitions* (Taylor & Francis, London, 1990), p. 41.
- <sup>21</sup>P. Kostic, Y. Okada, N. C. Collins, Z. Schlesinger, J. W. Reiner, L. Klein, A. Kapitulnik, T. H. Geballe, and M. R. Beasley, *Phys. Rev. Lett.* **81**, 2498 (1998).
- <sup>22</sup>Frederick Wooten, *Optical Properties of Solids* (Academic, New York, 1972).
- <sup>23</sup>H. G. Reik and D. Heese, *J. Phys. Chem. Solids* **28**, 581 (1967).
- <sup>24</sup>N. Shanthi and D. D. Sarma, *Phys. Rev. B* **57**, 2153 (1998).
- <sup>25</sup>David Emin, *Phys. Rev. B* **48**, 13 691 (1993).